Redundant and reconfigurable propulsion systems to improve motion capability of underwater vehicles

Redundant and reconfigurable propulsion systems to improve motion capability of underwater vehicles

Luca Pugi[*], Benedetto Allotta, Marco Pagliai

Dept. of Industrial Engineering, University of Florence, Florence, Italy

A B S T R A C T

Inspection of offshore plants or harsh marine environments, requires underwater vehicles with high autonomy, performances and maneuverability. These features are deeply affected by the design of propulsion system. An accurate design of the propulsion system, involves the modelling of the response of propellers. In this work a reconfigurable propulsion layout for an inspection vehicle is presented. Performances of the proposed solution are evaluated and compared respect to the conventional one which is currently installed on benchmark test vehicle (the MARTA AUV from University of Florence). Proposed layout exhibit superior maneuvering performances that should be useful for the inspection of offshore plants and more generally for harsh operational conditions.

1. Introduction

In this work, the applicability of a reconfigurable propulsion layout for underwater vehicles for offshore operations will be investigated. The innovative layout proposed, visible in the scheme of Fig. 1, is characterized by an array of four low cost pivoted thrusters that can be easily customized and optimized with respect to operating and mission profiles. In particular, authors supposed that the angular position of each thruster around its pivot axis, is controlled by a servomotor.

In existing solutions available in literature, such as SmartE AUV, (Meyer et al., 2013; Ehlers et al., 2014), three pivoted thrusters are used to perform a holonomic control of the six degree of freedom of underwater vehicle.

* Corresponding author.
E-mail addresses: luca.pugi@unifi.it (L. Pugi), Benedetto.allotta@unifi.it (B. Allotta), pagliai.marco@gmail.com (M. Pagliai).

In this proposed study, authors want use four pivoting actuators to control the vehicle motion to improve the maneuverability, the efficiency and the failure robustness with respect to a traditional AUVs or ROVs.

In details, the work is organized as follows:

In Section 2, it's introduced Current State of the Art and definition of a benchmark vehicle and operating scenario.

In Section 3, it's described the design of an actuator unit according to chosen requirements. Description includes preliminary tests and simplified models adopted to identify main features of the prototype in terms of performances and efficiency. In particular Finite Element design of the actuator magnetic joint is explained in Section 4, while preliminary experimental activities to identify actuator performances are described in Section 5. Finally a Virtual Model of the whole system aiming to investigate the potential features of the proposed approach is described in Section 6.

Results in terms of comparison between the proposed innovative solution and the conventional one are finally shown in the last part of this work corresponding to Section 7.

2. Current state of art

This work is based on the experience acquired by authors in the prototyping of hybrid multi-role AUVs (Autonomous Underwater Vehicles) 'TIFONE' (Allotta et al., 2012, 2011, 2015a), and 'MARTA' (Allotta et al., 2015b; ARROWS Project), whose propulsion layout is shown in Fig. 2. In this vehicles, two rear propellers are used for standard-straight navigation and a certain number of tunnel thrusters are devoted to control orientation or to keep the vehicle hovering over an assigned target. Considering the high number of controlled independent actuators (six), fixed pitch propellers are adopted to simplify the control logic. This choice allows to reduce costs. Additional vantages are represented by increased modularity and reliability of the whole vehicle, thanks to use of simple and standard components for all actuated axis.

Usually, the resulting propulsion layout makes possible to control five degree of freedom, which are described according the classical SNAME notation, widely adopted in literature (Fossen, 1994): Surge Motion: longitudinal load X is the sum of the thrust delivered by the two rear propellers.

dopted symbols

x, y, z	displacements along the three coordinate axis (surge, sway, heave directions)
φ, ψ, θ	rotations angle respect to the three axis (roll, pitch, yaw, rotations)
u, v, w	speed along body constrained directions (surge, sway, heave)
X, Y, Z	resultant forces applied on the tree body constrained directions (surge, sway, heave)
K, M, N	resultant torques applied along the three body constrained axis (roll, pitch, yaw, rotations)
τ	vector of resultant forces and torques applied to the vehicle (six components, X, Y, Z, K, M, N)
β	Propeller advance angle

V_a, n   Propeller advance and rotational speed p,d
                Propeller Pitch and Diameter Q,T
                Propeller Torque and Thrust
J   Advance Coefficient
K_T, K_Q Thrust and Torque Coefficients
C_T, C_Q Modified (four quadrant) Thrust and Torque
                Coefficients
A_k, B_k, C_k, D_k parameters of the formula defining modified Thrust and Torque Coefficients C_T, C_Q

T_{ij} Thrust delivered in the i-th direction by the j-th thruster, in particular the i-th index should be equal to " p " (thrust projected on the x-y plane) or " c " (thrust component in the z direction, vertical direction); the j-th index identifies the thruster, since in the vehicle are installed four thrusters j should be a number from 1
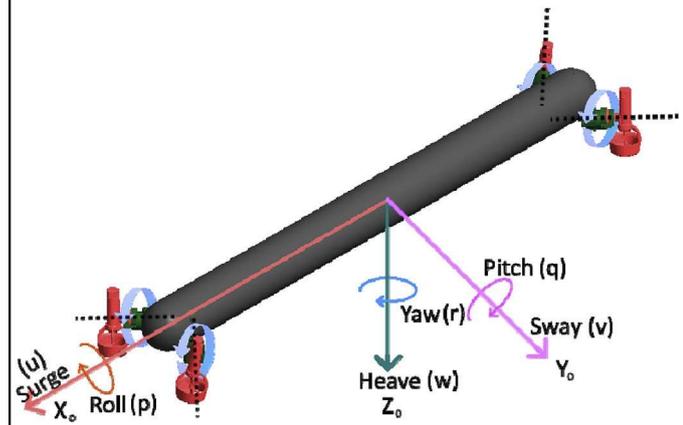

Fig. 1. Example of application with four orientable thrusters with SNAME notation.

           to 4
ω_i angular orientation/position of the i-th thruster along his pivot axis
l_{ij} are the distances between thruster axis respect to a body constrained reference system visible in Fig. 13. In particular the i-th index should be equal to " p " (distance projected on the x-y plane) or " c " (distance in the z direction, vertical direction); the j-th index identifies the thruster, since in the vehicle are installed four thrusters j should be a number from 1 to 4
H_i maneuverability index in the direction i
V_i speed of the vehicle in a generic direction i
W_i corresponding power need to move the vehicle in the i direction
Fig. 2. Marta AUV propulsion layout and corresponding encumbrances. Sway and

Heave: lateral load Y and Z are respectively the sum of the thrust of the two lateral and vertical Tunnel Thrusters.

Pitch and Yaw rotations: vertical and lateral thrusters respectively control these rotations. Yaw rotation has a redundant actuation, since it can be controlled also using the two rear propellers.
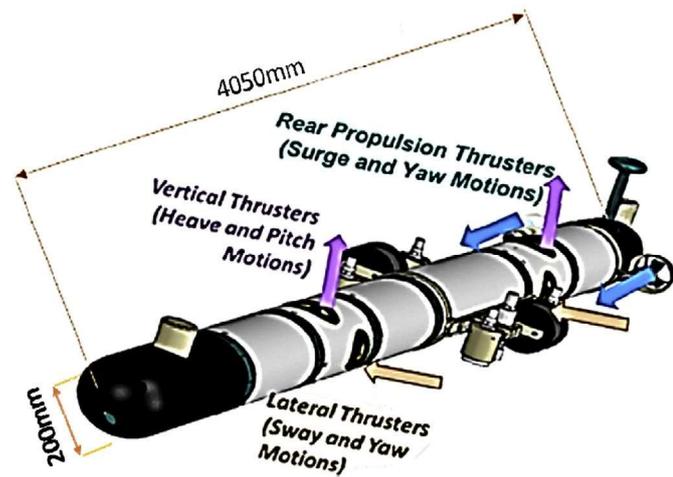
hull diameter). However, the total length of the three propulsion modules is more than 1.2 m. In addition, it should be noticed that over-cited

Table 1
Controlled and Uncontrolled Degree of Freedom for some typical Propulsion Layouts Adopted by commercial ROVS.

Heave	Controlled	Controlled	Controlled
Roll	Controlled	Not Controlled	Not Controlled
Pitch	Not Controlled	Not Controlled	Not Controlled
Surge	Controlled	Controlled	Controlled
Sway	Controlled	Controlled	Controlled
Yaw	Controlled	Controlled	Controlled

Roll rotation: usually is the only degree of freedom that is not controlled. The stability of this D.O.F is ensured by an appropriate choice of static weight and buoyancy distributions. Also fins should be used to further stabilize the vehicle respect to roll motions.

Many existing AUVs adopt similar combinations of fixed pitch rear propellers and lateral tunnel thruster to increase vehicle maneuvering. It is possible to cite many examples, such as C-Scout (Curtis et al., 2000), Remus (Stokey et al., 2005), Proteus (Whitney and Smith, 1998), Delphin2 (Phillips et al., 2009) and Folaga (Alvarez et al., 2009).

In this kind of layouts, the actuation of different degrees of freedom is highly decoupled, making quite easy the control of the vehicle. In addition, a wise choice of the propeller rotation sense can reduce the motion disturbances arising from propellers reaction torques. Also an easy controllability is an important requirement for the design of commercial ROVs (Remotely Operated underwater Vehicles), where the vehicle has to be maneuvered by a human operator, with a limited level of additional automation. Some examples of propulsion layouts often adopted on ROVs (or AUVs) are visible in Table 1.

Unfortunately, one of the drawbacks of the propulsion layout adopted on 'MARTA' or similar AUVs is the encumbrances of the propulsion system with respect to the payload. As shown in Fig. 2, the length of the MARTA Vehicle is about 4000 mm (about 18 times bigger with respect to
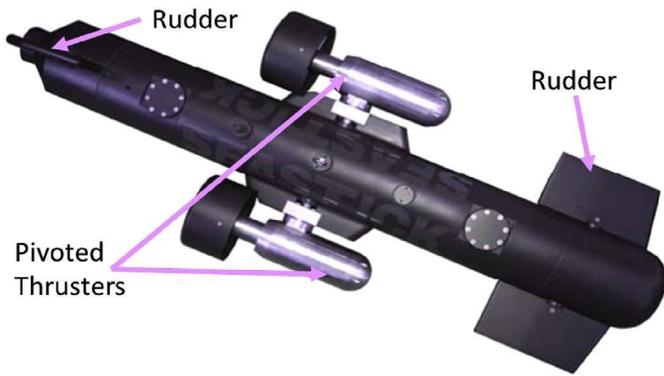
Fig. 3. Examples AUV-ROV with pivoted Thrusters (Faccioli, 2013).

propulsion layouts could not be dynamically reconfigured during the mission, so their use should be critical in scenarios with uncertain operating parameters, such as water density, currents, expected mission profile, availability or reliability of one or more actuators. For this kind of applications, the use of pivoted thrusters should be a cheap and reliable solution, as shown in some innovative commercial products, such as the Italian Sea-Stick (Faccioli, 2013), which is visible in Fig. 3.

In addition, pivoted thrusters have been recently used for research oriented vehicles such as the Smart E, developed by University of Lubeck, where three pivoted thrusters are used to control the six degree of freedom of spherical/saucer AUV (Meyer et al., 2013; Ehlers et al., 2014). 3. Design of pivoted thruster

Each pivoted thrusters, shown in Fig. 4, is designed to be a modular and independent units. Each thruster module is composed by an oil compensated thruster, a stepper motor, a magnetic joint, an oil refill system and some modular fixture elements. This particular structure aims to reduce cost and improve components standardization. In order to ensure this important features, authors decided to choose the oil compensated thruster, internally developed by authors. In particular this thruster is the same used for the propulsion of Marta (Allotta et al.,
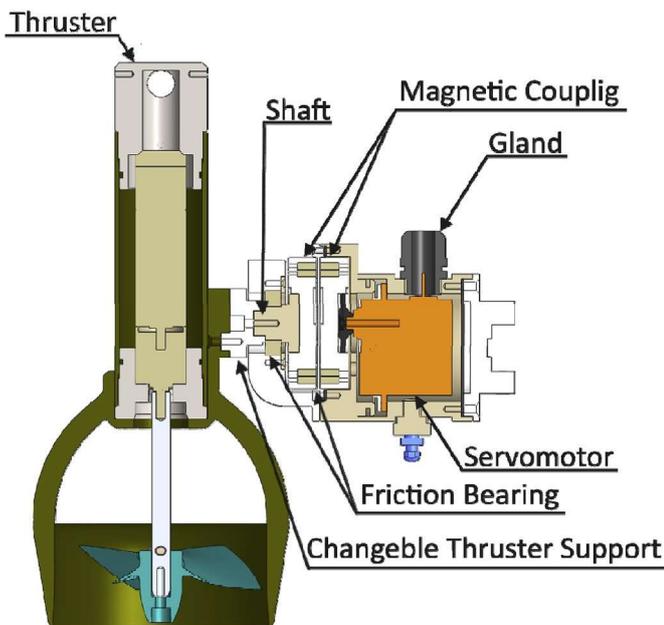

Fig. 4. Proposed pivoted thruster.

Name: HS-5646WP	
Alimentation [V]	6.0/7.4
Torque [Nm] (6.0 V/7.4 V)	1.11/1.26
Dimension [mm x mm x mm]	41.8 21.0 40.0
International Protection Code	IP67
Weight [g]	61

2015b) and Feel Hippo AUVs.

Orientation of the pivoted thruster is controlled using a servomotor. Authors chose a low cost commercial servomotor, whose main features are shown in Table 2.

The chosen servomotor is provided by the supplier with a waterproof case. This case it's not suited to resist to very high pressures and depths for which is designed the vehicle (100 m). So authors have to protect the servomotor with an additional case sealed and oil filled. Considering the double protection provided by the two concentric cases, the protection of the servomotor respect to the possibility of a contamination with salt water it's quite remote.

This choice was made to ensure a high reliability to the module. In this way, the motor can also tolerate water infiltrations. The primarily scope of the servomotor is to control the angular position of the thruster with respect to the hull frame. In this way it's possible control the orientation of the thrusters as request by the control system. In addition, in this case the servomotor, as the thruster, is oil filled in order to assure a good reliability with respect to different operating depths. The Servomotor is connected with the thruster using a magnetic coupling in order to protect the system against torque overload and water contamination.

Looking at the scheme of Fig. 4, the thruster is not directly connected to the shaft of the servomotor. In particular, an adjustable flange called "Changeable Thruster Support" is introduced. In this way it's possible to adjust both distance and angular position of the thruster respect to the servomotor by modifying the shape of the "Changeable Thruster Support".

The pressure compensation system consists in three simple components: the oil refill system, two compensation holes, and a compensation shell (Fig. 5). The oil refill system allows filling the servomotor case with the oil without air, otherwise compensation holes and compensation shell allows transferring the pressure of external water to the oil. This system allows using this pivoted thruster even at high depths.

For this activity, the more interesting aspects are related to the design of the magnetic coupling and more generally to the design of the sealed case of the position controlled motors which are described in detail in Fig. 4.

4. Magnetic coupling

Magnetic couplings and gears are used for applications involving low mechanical losses, maintenance-free operations, and inherent overload protection. In addition, for marine and hydraulic applications, the indirect coupling assured by magnetic joints is useful to reduce the risk of contamination of components like motors, which cannot be directly exposed to sea water.

As shown in Fig. 6, in order to couple the stepper motor with the thruster, it is possible to use both radial and axial magnetic joints. Both kinds of joints allow to transfer the torque thanks to electromagnetic interaction without the need of any mechanical link. In this work, after a preliminary design, it was preferred an axial solution in order to reduce the radial encumbrances.

The joint is designed with the aid of mathematical model, based on theoretical and empirical relationships developed by Furlani (1997, 2001). From these relationships, it was argued that the only way to produce a coupling
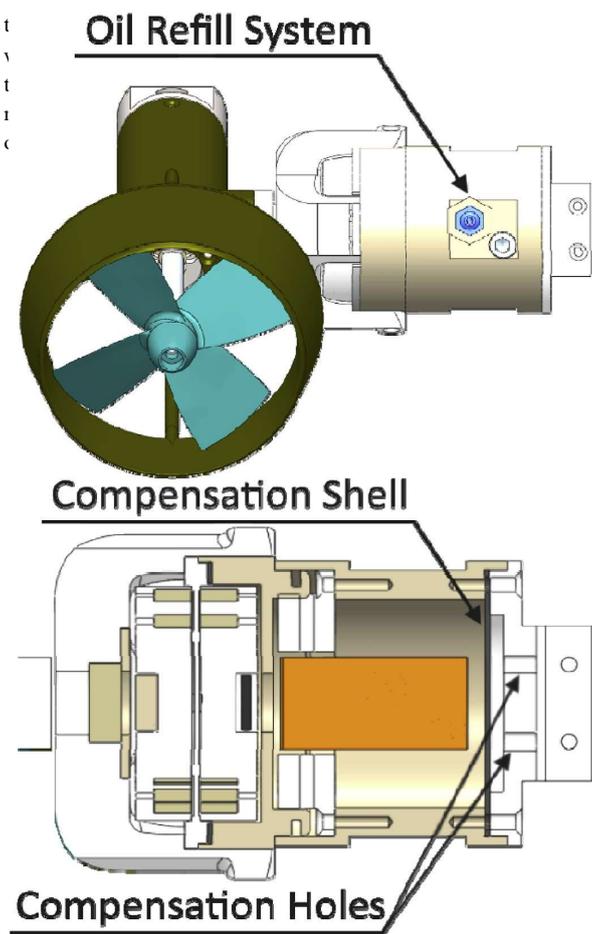
Oil Refill System
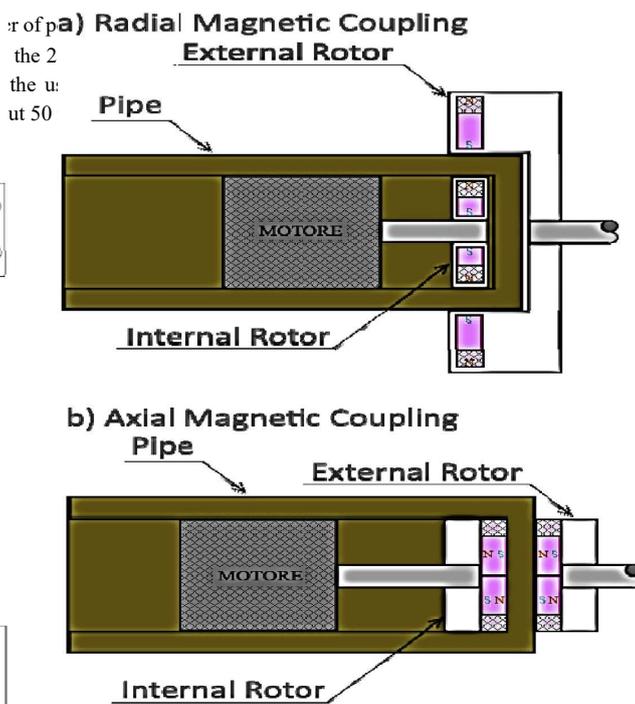

Fig. 5. Pivoted Thruster, detail of the pressure compensation system.

a) Radial Magnetic Coupling

b) Axial Magnetic Coupling

Fig. 6. Type of magnetic couplings.

Table 3
Many physic properties of used magnets.

Type	Coercive Force				Max Temperature
	bHc		iHc		
	kOe	kA/m	kOe	kA/m	C
N48	10.8 12.5	860 995	12	955	80

In order to easily build the joint and reduce costs, magnetic coup[ling] is assembled using arrays of smaller commercial magnets (magnets specifications are visible in Table 3). For this reason, Furlani's equations, which are defined for ideal geometries and conditions, cannot be exact[ly] verified in a real full scale prototype. So the design of the joint [is] further refined using a full 3D FEM model, visible in Fig. 7 the model was useful to understand the optimal layout of elementary cylindrical m[ag]nets in order to obtain the transmission of the target torque (about 1 [Nm]) with the assigned air-gap (2 mm) obtaining a high stiffness (a j[oint] compliance of 0.3 0.5). In particular, the Finite element model is fundamental to evaluate the effects of the complex geometry of the a[rray] of cylindrical magnets used for the assembly of the real system.

The goal of the design has been the realization of a smallest magn[etic] coupling able to convey at most about 75% of max torque of the se[rvo] motor, to protect the servo from overload. These constraints led to rea[lize] a joint composed by a large number of small magnets, with a diamet[er of] 57 mm and with the capability to convey about 1 Nm of torque. Comp[lete] features of the joint are summarized in Table 4

Finally, the performances of the joint was exercising the experi-mental test rig, as shown in Fig. 8

A mechanical interface is used to apply a known measured torque and to measure the corresponding displacement angle.
of best magnets layout (relative angular displacement of about 0.5).

The joint is composed by Elementary Neodymium Cylindical Magnets

Magnetic Flux in the mean of the airgap

Fig. 7. FEM model

Max Torque [Nm]	~1

Table 4
Magnetic coupling specifications.

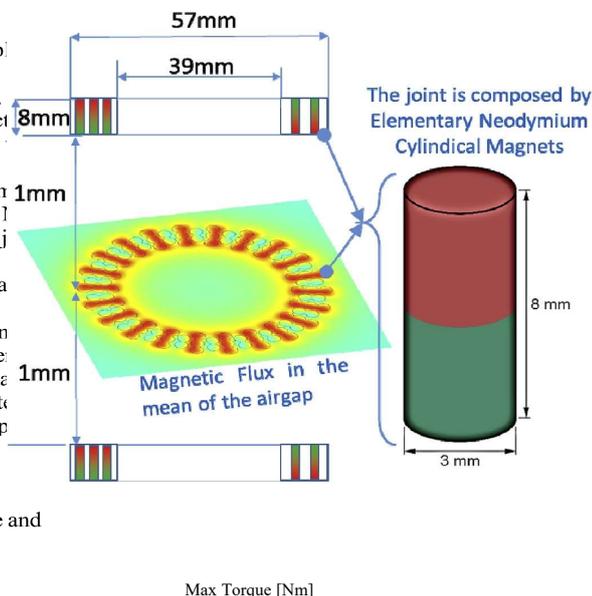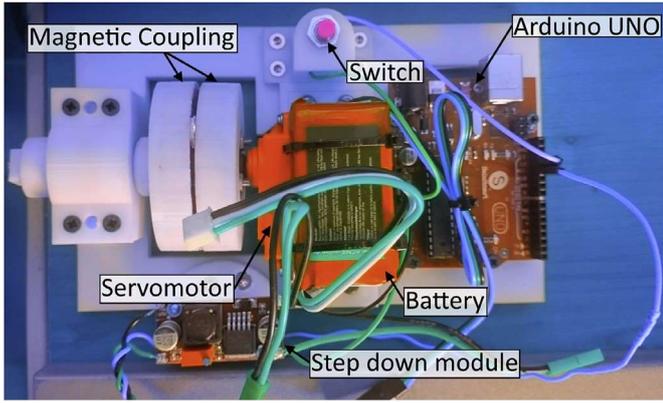|	
Number of magnets	220
Magnets diameter [mm]	3
Magnets height [mm]	8
External joint diameter [mm]	57
Joint height [mm]	26
Poles number	44
Joint air gap [mm]	2

Fig. 8. Experimental layout adopted for testing the magnetic coupling.

5. Preliminary identification of propeller behavior to four quadrants operation

For a proper design of the whole propulsion system, the behavior of the thruster has to be identified. Adopted thrusters is endowed by a standard Ka 4-70 propeller ducted with a 19-A convergent nozzle with a p/d ratio of 1.4 and a diameter of 90 mm. Since the same thruster have been previously adopted also for the propulsion of MARTA AUV, authors know performances of the thruster and the preliminary identification of the propeller through bollard thrust tests executed in the pool of MDM lab (Pistoia Italy). These tests provide some data used to extrapolate the propeller behavior and simulate four quadrants operations.

During these tests, executed with the simple device, described in Fig. 9, it was possible to identify power consumption, torque (Q) and delivered thrust (T) of propeller in static/bollard conditions (Allotta et al., 2015b).

In particular, as visible in Fig. 9, the tested thruster is constrained with load cells in order to estimate applied T and Q from the measurement of corresponding reaction forces: longitudinal motion of the
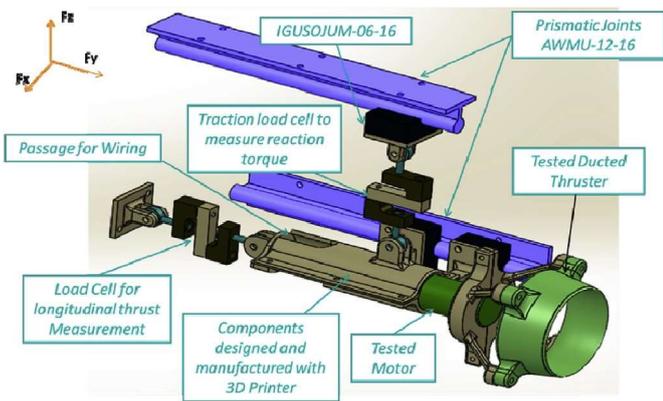

Fig. 9. Simplified scheme of test rig adopted for the measurement of bollard thrust.

thruster is avoided by a cheap load cell mounted on spherical joints, so measuring the force exerted on the cell is possible to directly evaluate the longitudinal effort of the propeller. A second cell, also mounted on spherical joints, is able to transmit and measure only the transversal reaction force due to transmitted torque. Knowing this reaction force (measured by the load cell) and the leverage distance it's possible to evaluate the corresponding reaction torque

which is almost equal to the torque delivered to the propeller. This testing layout was derived from previous experiences (Allotta et al., 2009; Pugi et al., 2016), of authors in the estimation of forces from corresponding measurements of reaction ones. Proposed measurement system is quite cheap and reliable since it's based on low cost traction-compression load cells. Also the system can be easily scaled for different measurement ranges since adopted load cells are a widely diffused commercial products that can be easily customized for a wide variety of sizes.

The study of four quadrants operations of the propeller is quite difficult. These difficulties are related to the possible zero value or the sign inversions of advance speed (V_a [m/s]).

In these conditions the rotational speed (n [Hz]) leads to a numerically inconsistent description of most commonly used parameters such as advance coefficient (J), thrust and torque coefficients (K_T and K_Q) (Carlton, 2007; Pivano et al., 2009). For this reason, propeller advance is expressed in terms of advance angle β (defined according (1)), where the advance speed V_a is scaled with respect to the propeller tangential speed calculated at the 70% of the propeller tip radius:

$$\beta = a\tan\left(\frac{V_a}{0.7\pi n d}\right)$$

By defining the β parameter, it is possible to redefine thrust and torque coefficients. New parameters are named C_T (2) and C_Q (3) and are respectively defined as thrust (T) and torque (Q) coefficients. They are scaled respect to kinetic energy associated to the inlet relative speed also referred to the 70% of the propeller tip radius:

$$C_T = \frac{T}{\frac{1}{8}\rho \overline{V_a^2} (0.7\pi n d)^2 d^2} \tag{2}$$

$$C_Q = \frac{Q}{\frac{1}{8}\rho \overline{V_a^2} (0.7\pi n d)^2 d^3} \tag{3}$$

C_T and C_Q coefficients are typically approximated in terms of Fourier series (4), (5).

$$C_T = \sum_{k=0}^{20} A_k \cos(k\beta) + B_k \sin(k\beta) \tag{4}$$

$$C_Q = \sum_{k=0}^{20} C_k \cos(k\beta) + D_k \sin(k\beta) \tag{5}$$

For the chosen propeller Ka 4-70 coefficients A_k, B_k, C_k, and D_k are known from literature (Oosterveld, 1970, 1973), and experimentally verified, by authors (Allotta et al., 2015b).

In particular, Fig. 10 shows the behavior of the modified coefficient C_T with respect to β: results of bollard thrust tests are obtained with values of β equal to 0 (forward thrust) and π (reversed thrust).

6. Development of a virtual model of the vehicle

Authors developed a virtual model of the vehicle in the Simscape™ environment of Matlab™ to test the new vehicle layout, visible in Fig. 1, and to compare it with the original MARTA layout, used as a benchmark/ reference test case.

The conventional propulsion layout of Marta corresponds to the scheme of Fig. 2 in which six thrusters are installed: two rear propeller, two vertical thruster, and two transversal ones. To perform the
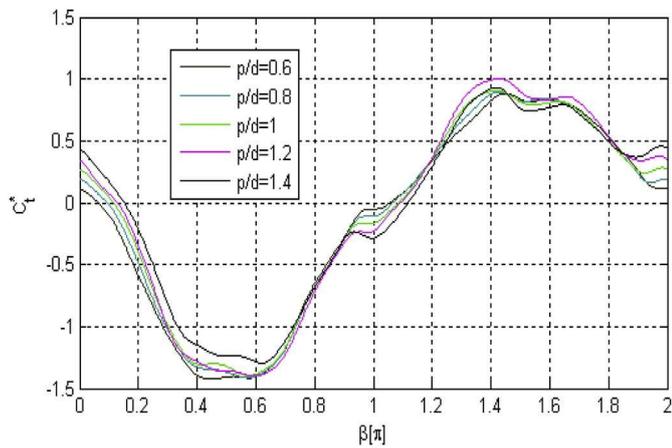
Fig. 10. Ct for a Ka 4-70 Propeller ducted on a 19-A nozzle, according to Oerstveld (Oosterveld, 1970).

Table 5
Motor and propeller specifications.

Property	Value	Property	Value
Motor Model	Maxon 386676	Nom. Voltage	18[V]
No-load Speed	31,000[rpm]	Nom. Current	9.11[A]
Nominal Speed	28,300[rpm]	Nom. Torque	0.049[Nm]
Speed Constant	1730[rpm/V]	Gearbox red. ratio	1/9.8
Propeller diameter	90[mm]	Propeller p/d	1.4
Propeller Type	KA 4-70	Nozzle	19-A

comparison, it's assumed that all the considered thrusters are equal. In particular data of the considered thrusters are shown in Table 5.

Since the maximum power of each thruster is about 150 W, the conventional layout (six thrusters) involves a total installed power of about 900 W, while the new one only 600 W (power absorbed by servomotors to control orientation is quite negligible respect to the thruster one).

In order to easily build both models, authors choose an extremely modular structure, as shown in Fig. 11a (which is referred to the model of the innovative solution proposed in this work), based on standard block that can be easily assembled and customized.

Same modular subsystems are used to also to assemble the model of the conventional propulsion layout visible in Fig. 11b.

All the models and sub-models described in Fig. 11a and b were written using Simulink-Simscape™ blocks.

As example, in Fig. 12 it's represented the implementation of the submodel describing Hull dynamics: the dynamics of the hull is calculated considering forces exerted by connected servomotors and thrusters blocks. The hull is also subjected to forces due to the interaction with the surrounding water. This Hydrodynamic forces are evaluated using the typical approach proposed by Fossen (1994) which considers the following contributions:

Drag Forces: the hull is subjected to viscous drag resistances due to friction with surrounding water (block Drag Forces in Fig. 12);

Added Mass Terms: the movement of the hull in the water causes additional motions of fluid which are equivalent to added inertial terms whose effects are modelled in the block "Added Mass Terms" visible in Fig. 12.

Static forces due to buoyance: it's possible to evaluate the hydrostatic lift forces calculated according the well-known principle of Archimedes. These forces are calculated in the block, called "Buoyant Force" in Fig. 12.
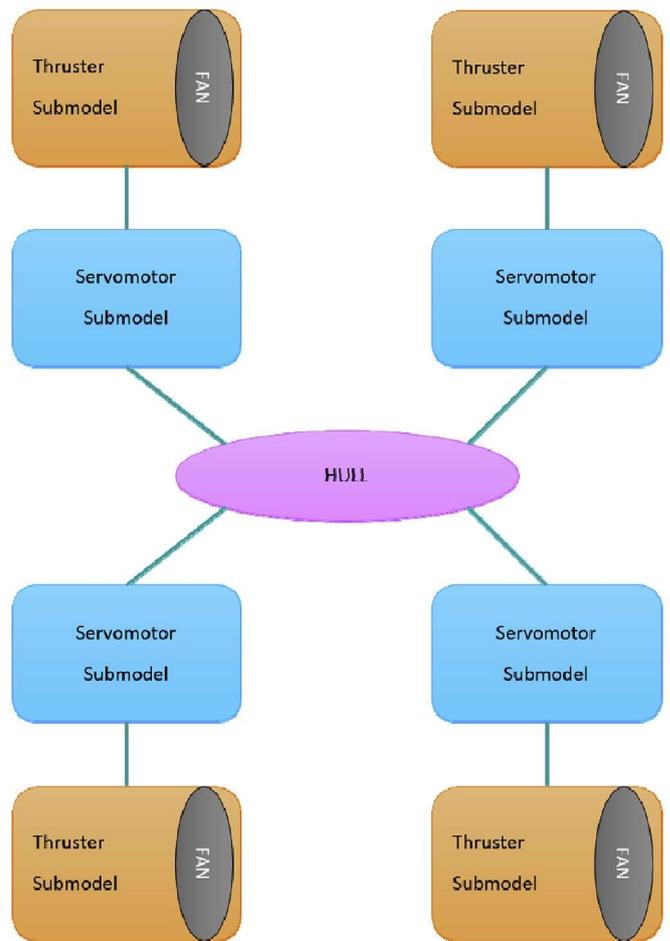
a
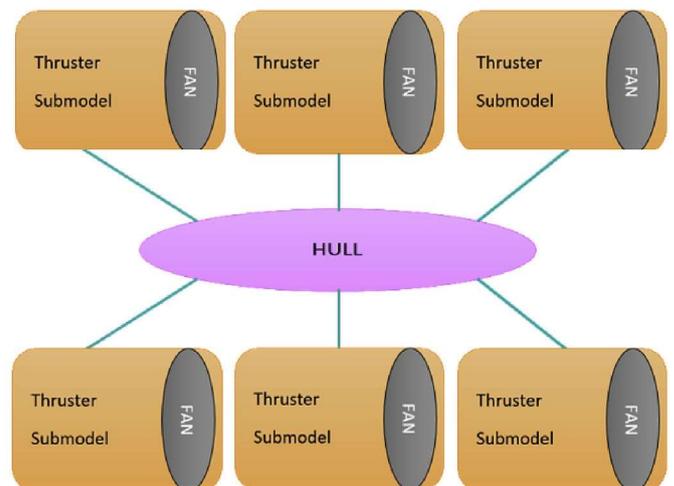
b

Fig. 11. a: scheme of connected subsystems for the model of the innovative propulsion layout considered in this work. b: scheme of connected subsystems for the model of the conventional propulsion layout of Marta.

Drag Forces

Added Mass Terms

Forces from connected
Servomotors and
Thrusters Blocks
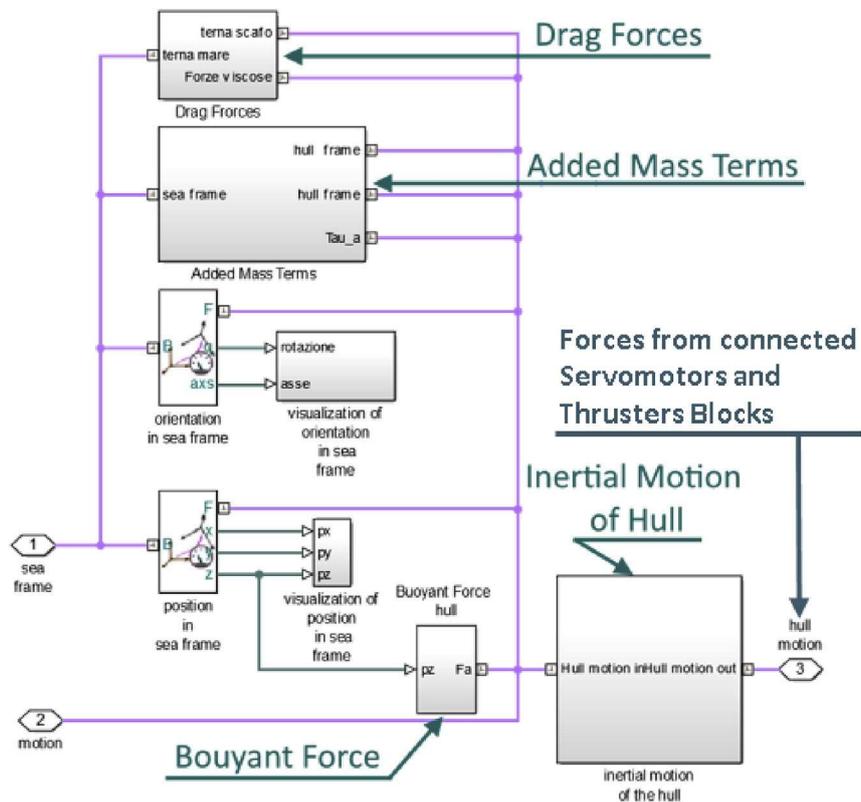
Inertial Motion
of Hull

Bouyant Force

Fig. 12. Example of a sub-model of the HULL (Simscape Implementation).

Inertial Terms: finally, the hull has its own inertial properties (mass, position of the center of mass, matrix of rotational inertial terms). Gravitational and inertial forces applied to the hull are calculated in

this block using standard multibody blocks available in SimulinkSimscape™. This functionality is implemented in the block called "Inertial Motion of the Hull" in Fig. 12. This block solves the multibody dynamics of the hull including contribution of gravitational forces.

In order to control the vehicles to test their performances, authors had to define an appropriated control logic. For this application, authors chosen for both models a decoupled control.

This solution is based on SISO (Single Input, Single Output) control systems with PID (Proportional-Integral-Derivative) controller for each degree of freedom of hull. Therefore, the six commands to actuators are obtained thanks to the allocation matrix described in Equation (6).

The dimension of matrix is equal to 8 6.

$\frac{1}{4}$ c$_{qpc4}$ l$_{c4}$
sin$\eth\omega_4$Þ

sin$\eth\omega_2$Þ 0 sin$\eth\omega_3$Þ 0$_0$sin$_{cos}\eth\eth\omega\omega_{44}$ÞÞ
cos$\eth\omega_2$Þ 0 cos$\eth\omega_3$Þ

τ ¼ 66666Z$_K$ 77777 ¼

0   m$_{35}$ m$_{45}$ l$_{p4}$
0   1   0 1
m$_{33}$ l$_{b2}$

246X$_{NM}$Y 357   m$_{34}$

26666664cos0$_m$sin$_m$l$_{p13141}$$\eth\eth\omega\omega_{11}$ÞÞ   l$_{b3}$ m$_{43}$

1$_C$00$_{qc}$l$_{ba111}$ l$_{a2}$

m$_{44}$

l$_{a3}$

l$_{p2}$ C$_{qc2}$ l$_{p3}$
C$_{qc3}$

with :
m$_{31}$ ¼ c$_{qps1}$ l$_{c1}$ cos$\eth\omega_1$Þ m$_{33}$ ¼   m$_{41}$ ¼ c$_{qpc1}$ þ
c$_{qps2}$ þ l$_{c2}$ cos$\eth\omega_2$Þ m$_{34}$ ¼ c$_{qps3}$ l$_{c3}$ l$_{c1}$ sin$\eth\omega_1$Þ
cos$\eth\omega_3$Þ m$_{35}$ ¼ c$_{qps4}$ l$_{c4}$ cos$\eth\omega_4$Þ   m$_{43}$ ¼ c$_{qpc2}$ þ
l$_{c2}$ sin$\eth\omega_2$Þ
m$_{44}$ ¼ c$_{qpc3}$ l$_{c3}$
sin$\eth\omega_3$Þ m$_{45}$

2T$_{p1}$3

0 7766T$_{p2}$

$$\begin{array}{l} 0 \quad 3\,T_{c1}\,7777^{777} \\[2mm] 1 \\ 666T_c{}^{p2}\,l^{b}4 \\ 77\ T\ ^3 l_{a4} \\ 7_7{}^6 6T\ _3 \\ c_{qc4}\ 5666T_{pc4}7775 \\[2mm] \qquad 4T_{c4} \end{array} \tag{6}$$

The parameters in relation (6) are shown in Fig. 13.

c_{qps1}, c_{qps2}, c_{qps3}, c_{qps4}, c_{qpc1}, c_{qpc2}, c_{qpc3}, c_{qpc4}, c_{qc1}, c_{qc2}, c_{qc3}, c_{qc4} are parameters necessary to model effects of torques generated by propellers on motors axes.

The usage of Allocation matrix involves the knowledge of eight components of motor actions. So it is necessary to define the corresponding four motor thrusts and four motor orientation angles. In this application, authors decided to obtain motors angles as arctangent of the ratio between corresponding T_p e T_c for each motor. Instead, motors thrusts are calculated as the module of the corresponding vector $j\,T_p\,T_c\,j^T$.

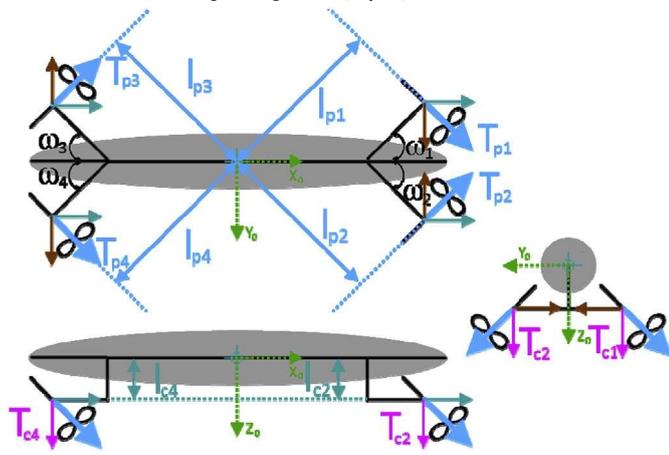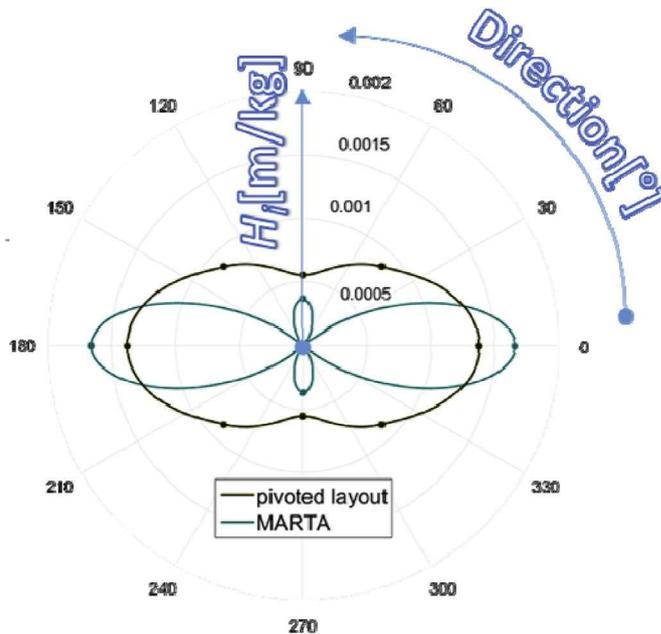Fig. 13. Scheme of pivoted layout.

7. Results

In order to compare the maneuverability of two examined vehicles, authors had to define an appropriate parameter named maneuverability. This parameter was defined as the inverse of the power consumption of motors normalized with respect to third power of the velocity of the vehicle (7). Finally, to realize a graphic representation of vehicles maneuverability in the horizontal plane, authors decided to represent results in a polar graphics, where the maneuverability was compared with respect to the direction of the velocity of the translational motion examined. In addition, simulations were realized with a reference velocity of 0.2 m/s, in order to compare different layouts avoiding scale effects.

$$\text{maneuvrability } H_i \frac{1}{4} \underline{\quad} \frac{V_i^3}{W_i} \ \text{m·kg}_1 \tag{7}$$

As shown in Fig. 14, the maneuverability of pivoted layout with respect to the maneuverability of original MARTA layout is extremely

increased. In particular it's far easier to control the vehicle during transversal or diagonal motions, still maintaining relatively good performances in longitudinal direction.

This condition it is due to the better use of motors in the pivoted configuration. In fact, the pivoted layout vehicle exploits constantly all thrusters simultaneously, whereby all motor running at low RPM. Conversely, ′MARTA′ can use only two thrusters to realize a single motion, whereby motors had to run at higher RPM, to push the vehicle at the same velocity of the proposed layout. Unfortunately, the improved motion capability involves a loss in maneuverability for what concerns forward translation, but the reduction of maneuverability is only about 17%, so it is not a penalizing condition. However, it is possible to tune this behavior, because the front section is related to ω_1, ω_2, ω_3 and ω_4 angles (Fig. 13). The comparison graph, shown in Fig. 14, was computed with all these angles equal to 45, but, if values of these angles is reduced, the maneuverability in forward direction increases and consequently lateral moving capability decreases. Conversely, if values of motor inclination angles decrease, lateral motion performances are privileged with respect to longitudinal ones. It is interesting to observe that this behavior can be exploited to properly tune the vehicle with respect to the operating conditions, as shown in Fig. 16.

Another interesting comparison is related to translations in the vertical direction. In this case, buoyancy forces and structural differences between two layouts heavily influence the comparison. This particular condition entails that the maneuverability of two layouts are comparable, when vehicles go down, but when vehicles go up, the maneuverability of pivoted layout is about 36 time better than ′MARTA′. This condition is, probably, due to the better stability and capability to maneuver of the proposed layout. Indeed, the motion of ′MARTA′ involve additional loss of efficiency of tunneled thrusters, which turn to very high RPM to provide adequate motion corrections.

As previously mentioned, motors inclination angles influence the maneuverability of the vehicle.

In Fig. 15 are shown effects produced by two different layout configurations.
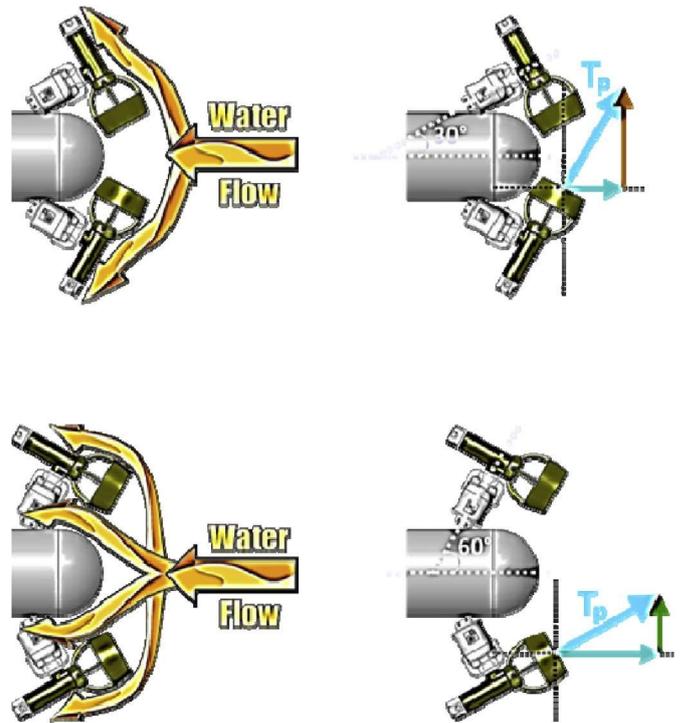

Fig. 14. Comparison between maneuverability of pivoted layout of the vehicle and maneuverability of MARTA.

Fig. 15. Comparison between pivoted layout with 30 angles and pivoted layout with 60 angles.

Different motors inclination angles involve the modification of fluodynamical features of the vehicle and the projection of motors actions in the vehicle plane.

In particular, smaller motor inclination angles, involve higher drag forces in longitudinal direction. Also smaller motor inclination angles produce lower thrust in longitudinal direction, but bigger in lateral one. As a consequence, smaller inclination angles, are associated to a better transversal maneuverability value and a worse longitudinal one.

In Fig. 16 these effects are clearly explained: with an angle of 60 maneuverability of the vehicle is similar to the Marta one. In fact, the maneuverability in longitudinal direction decreases only about 10% respect to Marta one.

In the transversal direction Maneuverability is only about 7% higher respect to the Marta one.

The great difference between these two layouts is the possibility to realize diagonal translations with the pivoted layout at 60. So it is possible to define the pivoted layout at 60 as the best compromise for standard mission requirements.

By reducing, the angle to 30 the vehicle performances in longitudinal and transversal directions are almost equivalent.

The pivoted layout not only offers improved maneuverability but also confers enhanced failure robustness. Indeed, three pivoted thrusters are enough to perform motion in 6 degrees of freedom. With the proposed layout, in case of a failure (failure of a thruster motor or a servomotor), the vehicle can move in an acceptable way, without losing any degree of freedom. Of course, the control logic has to be adapted to the failure but the vehicle conserve a backup functionality that should assure the autonomous return to home and consequently its recovery.

This particular feature of the system can be easily understood observing the structure of the allocation matrix in case of single fault: in case of failure of one of the four thrusters, two columns of the allocation matrix has to be removed. As example if the failed thruster is the number one the new 6 6 allocation matrix is described by system (8) which can be solved without losing the control of any degree of freedom.
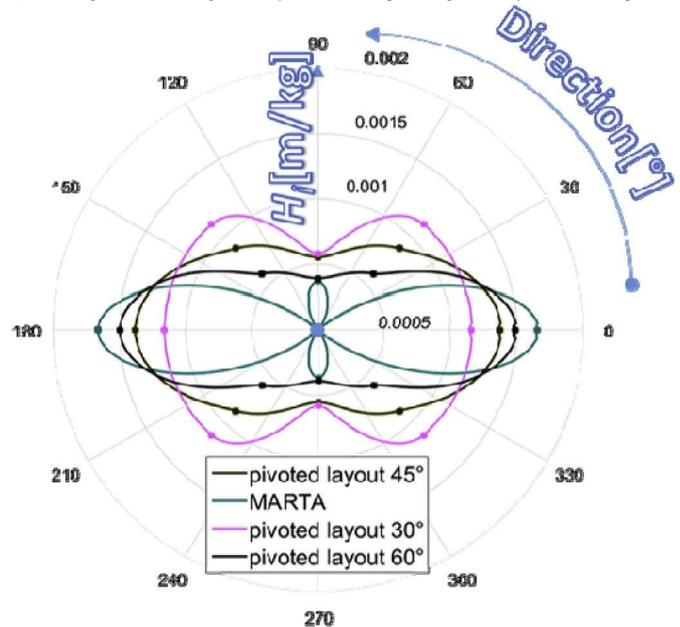

Fig. 16. Comparison between maneuverability of the proposed innovative layout and the conventional one for different angles.
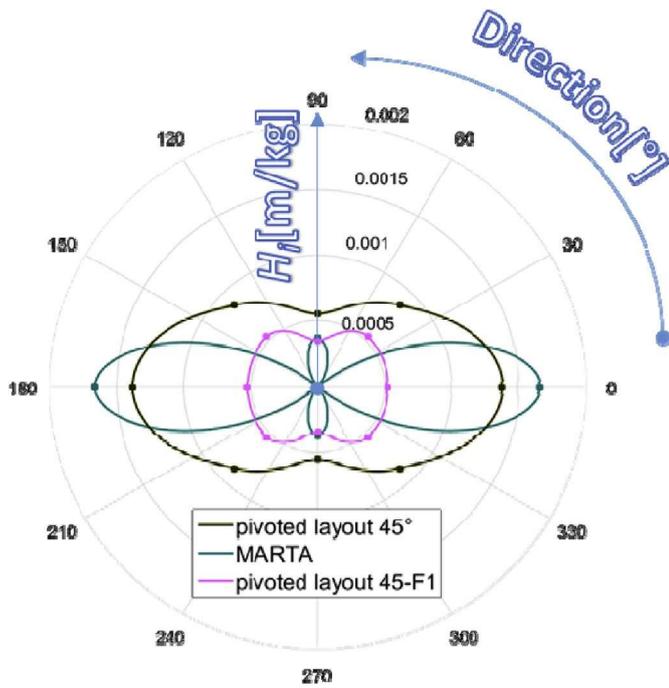
Fig. 17. Comparison between maneuverability of pivoted layout of the vehicle, maneuverability of pivoted layout whit a motor failure and maneuverability of MARTA.

$$2XY\ 3$$
$$6$$

$$\tau = 666664ZK_{MN}\ 7777775$$

$$2_{sincos}\eth\omega_2\triangleright\ 0 \qquad sin\eth\omega_3\triangleright\ 0 \qquad sin\eth\omega_4\triangleright\ 0\ 32_{Tp2}3$$

$$= {}^6 66 {}^6 m_{033p}\eth\omega_2\triangleright\ 1|0_{bqc2\ a}\ 0_{mcos_{p34}}\eth\omega_3\triangleright\ 10_{aqc|b3}\ 0_{mcos_{35p}}\eth\omega_4\triangleright\ 1|0_{abqc4}$$
$$7_{77}{}^7 76 {}^6 646 {}^6 6T_{TTTT_{ppccc24343}}\ 7_{77}{}^{77}75 \tag{8}$$

$$664_{m43|\ 2} \qquad c|_{22} \quad ml\ _{344} \qquad lc_{33} \quad m_{45|\ 4} \qquad cl_{44}57$$

Obviously, in these cases, the maneuverability of the vehicle decreases, but the AUV, keeps sufficient operating capability to complete the mission or to safely return to the base since it's still possible to control all the degree of freedom of the vehicle. As shown in Fig. 17, a failure causes a reduction of the maneuverability (referred to the case with 45of pivot inclination) in longitudinal direction of about 60%.

The corresponding reduction in transversal direction is lower, about 40%. Also in diagonal direction the reduction is limited to about 40%. It's interesting to notice that the damaged vehicle can be moved at lower speed but almost with the same performances in every direction.

8. Conclusions

The proposed solution exhibits better performances in terms maneuverability and hovering motions respect traditional AUV motors layout. This improvement results significant and involves a reduction of power consumption during navigation, allowing increase the length of missions. In addition, the proposed solution makes the vehicle more tolerant to failures since the propulsion layout is redundant: for the complete control of six degrees of freedom of the vehicle only three pivoted thrusters are needed, as in the case of Smart E AUV (Meyer et al., 2013; Ehlers et al., 2014). A minor drawback of a system with four independent pivoted thrusters is represented by the control logic which is a bit more complex respect to the conventional one. As final conclusion authors believe that benefit in terms of performances and robustness of the proposed solution justify its application on the real vehicle.

References

Allotta, B., Pugi, L., Bartolini, F., 2009. An active suspension system for railway pantographs: the T2006 prototype. Proc. Institution Mech. Eng. Part F J. Rail Rapid Transit 223 (1), 15–29. https://doi.org/10.1243/09544097JRRT174.

Allotta, B., Pugi, L., Costanzi, R., et al., June 2011. Localization algorithm for a fleet of three AUVs by INS, DVL and range measurements. In: Proceedings of the 15th International Conference on Advanced Robotics, 2011, Tallinn, vols. 20–23. IEEE, New York, pp. 631–636.

Allotta, B., Costanzi, R., Monni, N., Pugi, L., Ridolfi, A., Vettori, G., 2012. Design and simulation of an autonomous underwater vehicle. In: ECCOMAS 2012-European Congress on Computational Methods in Applied Sciences and Engineering, e-Book Full Pap, pp. 3656–3673.

Allotta, B., Pugi, L., Bartolini, F., Ridolfi, A., Costanzi, R., Monni, N., Jelli, J., 2015. Preliminary design and fast prototyping of an Autonomous Underwater Vehicle propulsion system. In: Proceedings of the Institution of Mechanical Engineers, Part M: Journal of Engineering for the Marit October 6, 0: 1475090215605133v1–1475090215605133.

Allotta, B., Costanzi, R., Gelli, J., Pugi, L., Ridolfi, A., 2015. Design of a modular propulsion system for MARTA AUV. In: Proceedings of OCEANS' 15 MTS/IEEE GENOVA, vols. 18–21. IEEE, Genova, Italia. ISBN: 978-1-4799-8736-8 maggio.

Alvarez, A., Caffaz, A., Caiti, A., Casalino, G., Gualdesi, L., Turetta, A., Viviani, R., 2009. Folaga: a low-cost autonomous underwater vehicle combining glider and AUV capabilities. Ocean. Eng. 36, 24–38 A.

Official web-site of the ARROWS project (Archeological robot systems for the world's seas) http://www.arrowsproject.eu/.

Carlton, J., 2007. Marine propellers and Propulsion, second ed. Elsevier.

Curtis, T.L., Perrault, D., Williams, C., et al., May 2000. C-SCOUT: a general-purpose AUV for systems research. Tokyo, Japan. In: Proceedings of the 2000 International Symposium on Underwater Technology 2000 (UT '00), vols. 23–26. IEEE, New York, pp. 73–77.

Ehlers, K., Meyer, B., Maehle, E., 2014. Full holonomic control of the omni-directional AUV SMART-E. In: Proceedings for the Joint Conference of ISR 2014-45th International Symposium on Robotics and Robotik 2014-8th German Conference on Robotics, ISR/ROBOTIK 2014, pp. 299–304.

Faccioli, A., June 2013. SeaStick AUV con funzionalita ROV. Oristano, Italy. In: Proceedings of Operational Oceanography, Innovative Technologies and Applications, vols. 3–5.

Fossen, T.I., 1994. Guidance and Control of Ocean Vehicles. Wiley. ISBN 0-471-94113-1.

Furlani, E.P., 1997. A two-dimensional analysis for the coupling of magnetic gears. IEEE Trans. Magn. 33 (3), 2317–2321.

Furlani, Edward P., 2001. Permanent Magnet and Electromechanical Devices: Materials, Analysis, and Applications. Academic Press.

Meyer, B., Ehlers, K., Osterloh, C., Maehle1, E., December 2013. Smart-e an autonomous omnidirectional underwater robot, paladyn. J. Behav. Robot. 4 (4), 204–210. https://doi.org/10.2478/pjbr-2013-0015. ISSN (Print) 2081-4836.

Oosterveld, M.W.C., 1970. Wake Adapted Ducted Propellers. Netherlands Ship Model Basin (NSMBPublication No. 345), Wageningen.

Oosterveld, M.W.C., 1973. Ducted propeller characteristics. In: RINA Symposium on Ducted Propellers, London.

Phillips, A.B., Steenson, L., Harris, C., Rogers, E., Turnock, S.R., Furlong, M., 2009 JanMar. Delphin2: an over actuated autonomous underwater vehicle for manoeuvring research,Trans RINA. Part A1, Intl. J. Marit. Eng. 151.

Pivano, L., Johansen, T.A., Smogeli, Ø.N., 2009. A four quadrant thrust estimation scheme for marine propellers: theory and experiments. IEEE T Contr. Syst. T 17 (1), 215–226.

Pugi, L., Galardi, E., Pallini, G., Paolucci, L., Lucchesi, N., 2016. Design and testing of a pulley and cable actuator for large ball valves. Proc. Institution Mech. Eng. Part I J. Syst. Control Eng. 230 (7), 622ˉ639. https://doi.org/10.1177/0959651816642093.

Stokey, R.P., Roup, A., von Alt, C., et al., September 2005. Development of the REMUS 600 autonomous underwater vehicle. In: Proceedings of MTS/IEEE OCEANS, 2005, Washington, DC, vol. 2. IEEE, New York, pp. 1301ˉ1304, 17ˉ23.

Whitney, J.W., Smith, S.M., 1998. Observations on the dynamic performance of tunnel thrusters. In: OCEANS'98 Conference Proceedings, vol. 2. IEEE.